Chapter in *Performance Characterization and Evaluation of Computer Vision Algorithms,* Proc. Dagstuhl Seminar, R. Klette, H.S. Stiehl, M. Viergever, and K. Vincken (Eds.), *Computational Imaging and Vision Series,* Kluwer Academic Publishers, Dordrecht Boston London 2000

PERFORMANCE CHARACTERIZATION OF LANDMARK OPERATORS

K. ROHR, H.S. STIEHL, S. FRANTZ AND T. HARTKENS
Universität Hamburg, FB Informatik, AB Kognitive Systeme
Vogt-Kölln-Str. 30, D-22527 Hamburg, Germany

1. Introduction

Prominent points in multi-dimensional digital images of different modalities are key features for a variety of computer vision tasks. As point landmarks we define, e.g., corners in 2D projection images or tips of anatomical structures in 3D spatial images, both of which are represented by geometric properties of the underlying intensity function. Note that, in the case of 3D spatial images, the geometry of the intensity function in general directly reflects the geometry of the depicted anatomical structures, which is generally not the case for 2D projection images.

In this chapter, we describe our studies on the performance characterization of operators for the detection and localization of point landmarks. First, we discuss the general problem as well as our approach to the validation and evaluation of landmark operators. Then, we detail our investigations for the case of 2D as well as 3D landmark operators.

2. General Approach to the Evaluation of Landmark Operators

As a methodical basis we adopt a general approach to the validation and evaluation of landmark operators. This approach consists of three principal steps as depicted in Fig. 1. Central to this scheme is the formalization of the signal structure which in our opinion is of paramount importance and is a key issue in the development of algorithms with predictable performance. Examples are the modelling of the systematic intensity variations in 2D projection images (see Section 3) or the modelling of structures in 3D tomographic images of the human brain (see Section 4). A prerequisite in the latter case is a careful analysis of brain anatomy. In either case, we have to

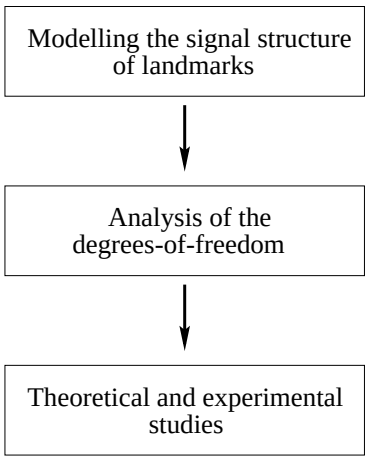

Figure 1. General approach to the evaluation of landmark operators.

find a mathematical description of geometric properties, e.g., in terms of differential geometry.

A second main step is a detailed analysis of the degrees-of-freedom. Here, a fundamental problem is that the number of the degrees-of-freedom are often very large. Particularly, this is true in the case of 3D landmark operators, where we can classify the degrees-of-freedom w.r.t. (i) anatomy (e.g., landmark type, scale, anatomical variability), (ii) imaging (e.g., contrast, noise, resolution, modality), as well as (iii) the algorithm (e.g., operator type, filter widths, thresholds). In experimental studies it is often possible to analyze the performance w.r.t. only a subset of the degrees-of-freedom. Priorities may be set on the basis of application scenaria, requirement analyses, and criteria catalogues comprising criteria such as accuracy, robustness, and reproducibility.

Third, theoretical as well as experimental studies should be performed. A theoretical assessment of operator performance should be strived for to a maximum extent, provided a mathematical treatment is possible at all. In addition, experimental studies are indispensable for performance prediction in real applications. To this end, we advocate an incremental approach building upon a hierarchy of test data (e.g., [16]). By this, we mean an experimental strategy that starts out from synthetic ideal signal structures of landmark prototypes and incrementally increases the complexity of the test data by incorporating, e.g., image blur, noise, different sampling schemes, and further degradations. The usage of synthetic images at first in comparison to real images has the advantage that 'ground truth' is available.

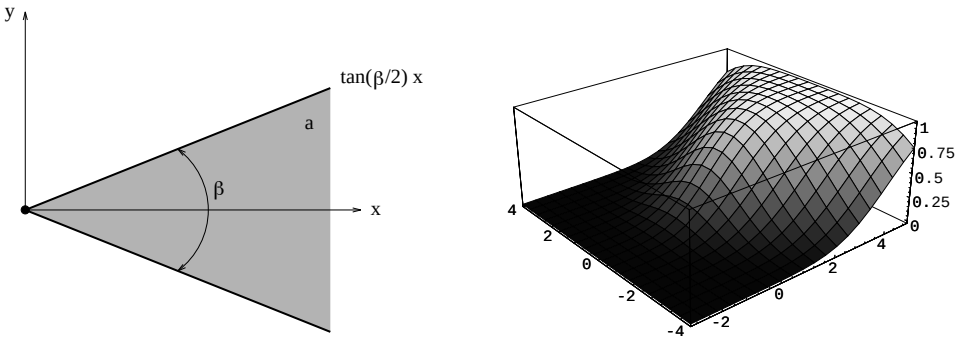

Figure 2. Model of an L-corner.

3. 2D Landmark Operators

In this section, we describe an analytic study to characterize the performance of operators for extracting 2D point landmarks. We consider corners of polyhedral objects and analyze the localization properties of ten well-known differential corner detectors. Note, that this study is not only relevant for 2D projection images but also for 2D slices of 3D tomographic images exhibiting similar tip-like structures. Our study is based on an analytic model of the intensities of an L-corner in [18],[19]. We have analyzed the dependence of the localization accuracy on all model parameters given the full range of the parameter values (Rohr [20]). Another analytic study of corner operators by Deriche and Giraudon [5] only considered specific aperture angles of an L-corner (45^o and 90^o) to compare three different operators. In alternative studies, the performance of corner operators has been investigated experimentally, either by visual judgment of the results (e.g., Kitchen and Rosenfeld [15]), by applying statistical measures (e.g., Zuniga and Haralick [26]), by using projective invariants (e.g., Coelho et al. [4], Heyden and Rohr [14]), or by computing the number of corresponding points under elastic transformations (e.g., Hartkens et al. [12]) and projective transformations of planar scenes (e.g., Schmid et al. [23]).

An L-corner can be modelled by Gaussian convolution of a wedge-shaped structure (see Fig. 2). Taking advantage of the symmetry of this structure, we can derive an analytic model which can be written as the superposition of two functions representing the upper and lower part of the L-corner, resp. ([19]):

$$g_{ML}(x, y, \beta, a, \sigma) = a \left(M(\frac{x}{\sigma}, \frac{y}{\sigma}, \beta) + M(\frac{x}{\sigma}, -\frac{y}{\sigma}, \beta) \right), \tag{1}$$

where β is the aperture angle, a the contrast, and σ quantifies the image

blur, while

$$M(x,y,\beta) = \phi(x,y) - \int_{-\infty}^{x} G(\xi)\ \phi(t\xi - \zeta_2)d\xi, \tag{2}$$

with

$$\phi(x,y) = \phi(x)\phi(y), \qquad \phi(x) = \int_{-\infty}^{x} G(\xi)d\xi, \qquad G(x) = \frac{1}{\sqrt{2\pi}} e^{-\frac{x^2}{2}}, \tag{3}$$

and $t = \tan(\beta/2)$, $\zeta_2 = tx - y$.

For this model we have analyzed the localization accuracy of ten differential operators ([20]). It turned out that some of the operators are either equivalent or do not yield any point. For the remaining six operators, the localized corner points are independent of the contrast, i.e. $x(a) = const.$, but there is a linear dependence on the image blur, i.e. $x(\sigma) = x \cdot \sigma$. Note, that since we have a symmetric structure the localized points lie on the x-axis (cf. Fig. 2) and therefore we only have to compute the positions along this axis. The dependence on the aperture angle, $x(\beta)$, is nonlinear and is depicted in Fig. 3 for the whole range of $0^o \leq \beta \leq 180^o$ while choosing $\sigma = 1$. From this figure we see that the operator of Beaudet [1] yields two positions for the corner model (denoted by x_{Bp} and x_{Bn} and represented by the solid curves). The other operators yield only one position and are abbreviated and depicted as follows: Dreschler and Nagel [6] by x_{DN} and the solid curve, Kitchen and Rosenfeld [15] by x_{KR} and the boldfaced dashed curve, Förstner [8] by x_F and the dashed curve, Rohr [17] by x_R and the dotted curve, and Blom et al. [3] by x_{BRK} and the dashed dotted curve. It can be seen that the localization accuracy strongly depends on β. For $\beta = 90^o$ most operators have a localization error to the tip of the unblurred structure of about $1pix$, where pix denotes spatial unity. For smaller values of β we have significantly larger errors.

As additional reference position we have also computed the positions of the (exact) curvature extremum along the Canny edge line (denoted by x_L and represented by the bold-faced curve). Although the differential operator corresponding to this definition is rather extensive, we can derive a relatively simple equation which determines its positions. With $x' = x/q$, $q = \sqrt{1+t^2}$ and $t = \tan(\beta/2)$, this equation can be stated as ([19]):

$$G(x') - t^2 x' \phi(x') = 0, \tag{4}$$

which is an implicit equation involving the aperture angle β. Also in this case the positions are independent of the contrast a and there is a linear

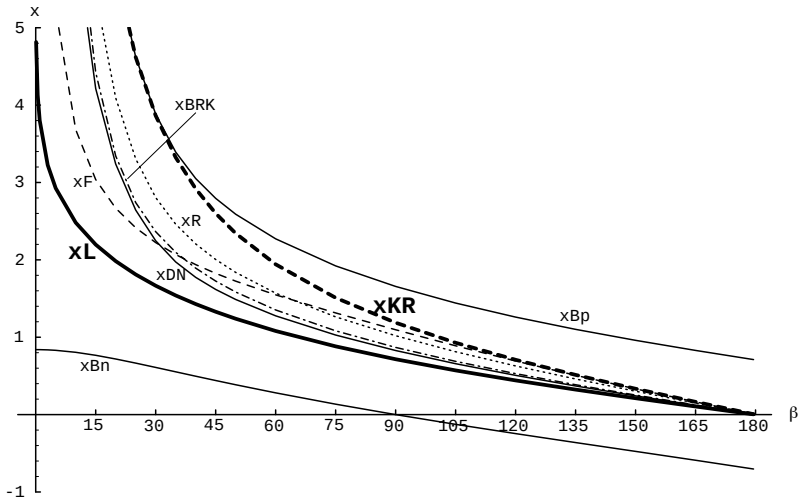

Figure 3. Localization of different 2D corner operators as a function of the aperture angle β of an L-corner with an image blur of $\sigma = 1$.

dependence on the image blur σ. From Fig. 3 it can be seen that the dependence on β qualitatively agrees with that for the corner operators discussed above.

Recently, we have shown analytically that the localization errors of differential corner operators can significantly be reduced by applying multi-step approaches (Frantz et al. [10]). Note also, that a model-based approach to the localization of corners (Rohr [18],[19]) allows to determine the correct position independently of all three parameters β, a, and σ.

4. 3D Landmark Operators

In the case of 3D landmark operators, we consider the extraction of anatomical point landmarks in tomographic images of the human brain. Generally, these landmarks serve as features for the registration of 3D multi-modality image data (e.g., MR and CT images as well as digital atlases). Thirion [25], for example, has introduced 3D differential operators to detect extremal points on ridge lines. These operators employ partial derivatives of an image up to the third order. However, the computation of high order partial derivatives generally is rather sensitive to noise. Related ridge-line based operators as well as operators based on the mean and Gaussian curvature using partial derivatives up to the second order have been investigated in [2] (see also, e.g., [7]). Rohr [21] has introduced 3D differential operators which are generalizations of existing 2D corner detectors. These operators employ either only first order partial derivatives or first and second order partial derivatives of an image. Therefore, these operators are computa-

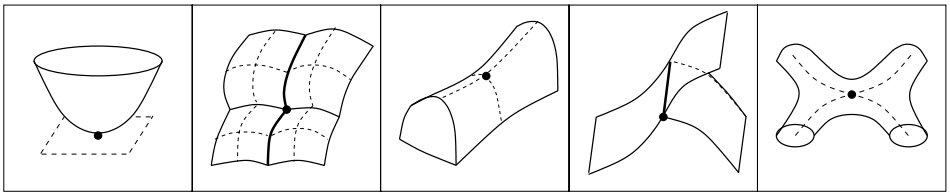

Figure 4. Different types of 3D point landmarks.

tionally efficient and they do not suffer from instabilities of computing high order partial derivatives. All operators mentioned above have only been designed for landmark detection and yield voxel positions. Recently, we have also proposed multi-step differential approaches for refined localization of 3D landmarks which yield subvoxel positions (Frantz et al. [10]).

To assess the performance of the different 3D operators we have carried out several studies. These studies include investigations of the localization accuracy as a function of image blur and noise, as well as the application of statistical measures to quantify the detection performance. The studies are based on 3D synthetic data (e.g., tetrahedra and ellipsoids), where ground-truth is available, as well as on 3D tomographic images of the human brain (MR and CT images). The basis of our evaluation studies is a detailed analysis of brain anatomy resulting in a geometric characterization of point landmarks (Rohr and Stiehl [22]). Examples of different classes of point landmarks are shown in Fig. 4. It appears that many point landmarks can be classified as either tips or saddle points (e.g., the tips of the ventricular horns or the saddle point at the zygomatic bone). In the following, we focus on these types of landmarks. Other types of landmarks are, for example, surface-surface and line-surface intersections (e.g., junctions of sulci) or center points of cylinder crossings (e.g., optic chiasm).

4.1. EVALUATION OF 3D DETECTION OPERATORS

We have investigated nine different 3D differential operators for detecting anatomical point landmarks in 3D images $g(x, y, z)$. Since most of these operators are 3D extensions of 2D corner operators we denote them by the names of the corresponding authors who introduced the 2D operators. Three of the nine operators are based on the mean curvature H of isocontours, two operators are based on the Gaussian curvature K, and one exploits the Hessian matrix $\mathbf{H}_g$. Another three operators are based on the matrix $\mathbf{C}_g = \overline{\nabla g\,(\nabla g)^T}$, which is the averaged dyadic product of the image gradient $\nabla g = (g_x, g_y, g_z)^T$. In summary, we have the following nine 3D operators: H, *Kitchen&Rosenfeld3D* $= H \cdot 2|\nabla g|$, *Blom3D* $= H \cdot 2|\nabla g|^3$, K, $K^* =$

$K \cdot |\nabla g|^4$, $Beaudet3D = det\mathbf{H}_g$, $Op3 = det\mathbf{C}_g / trace\mathbf{C}_g$, $Rohr3D = det\mathbf{C}_g$, $Förstner3D = 1/trace\mathbf{C}_g^{-1}$ (see also [21],[13]).

The detection performance of these operators has been assessed on the basis of statistical measures using 3D synthetic data as well as 3D MR and CT images (Hartkens et al. [13]). Alternative studies are based on the number of matched points in rigid ([25]) or elastic ([13]) registration, or determine the rigid or affine registration accuracy (e.g., [25],[2]). In a previous study, we compared the performance of the operators based on the mean and Gaussian curvature with ridge-line based operators (Beil et al. [2]). Analyzing the localization accuracy as a function of blur and noise, the number of false detections as a function of the size of the region-of-interest (ROI), and the affine registration accuracy, we found that the operator K^* from above yielded the best result together with the ridge-line based operators (which are computationally more expensive). Therefore, we did not consider ridge-line based operators in the present study.

To compute statistical measures for the detection performance, we consider around each landmark a ROI ($25 \times 25 \times 25$ voxels) as well as a detection region ($7 \times 7 \times 7$ voxels). The usage of a detection region has the advantage that small localization errors of the operators (cf. [20],[10]) do not falsify the detection performance. The measures used in our study are based on the following quantities: n_d as the overall number of detections, $n_{d,in}$ as the number of correct detections (detections inside the detection region), n_l as the overall number of landmarks, and $n_{l,detect}$ as the number of landmarks with at least one detection inside the detection region. Based on these quantities we compute the following measures for the detection performance:

$$P_{in} = \frac{n_{d,in}}{n_d}, \qquad P_{detect} = \frac{n_{l,detect}}{n_l}, \qquad P_{multiple} = \frac{n_{d,in}}{n_l}, \tag{5}$$

which quantify the fraction of correct detections, the fraction of detected landmarks, and the average number of multiple detections per landmark, resp. Previously, statistical measures have been applied in the case of 2D corner operators (e.g., Zuniga and Haralick [26]). However, only two measures have been employed there and detection regions around corners have not been considered. Thus, the resulting detection performance in that work depends more strongly on the localization accuracy.

In the case of 3D synthetic images (tetrahedra, ellipsoids, hyperbolic paraboloids), we have analyzed the measures in (5) as a function of the parameters of the modelled landmarks as well as the noise level. In the case of 3D MR and CT images, we have computed the mean values of the measures for all considered landmarks (see Fig. 5 for the case of MR images). In total, we have analyzed 242 synthetic and 43 real images, where image here

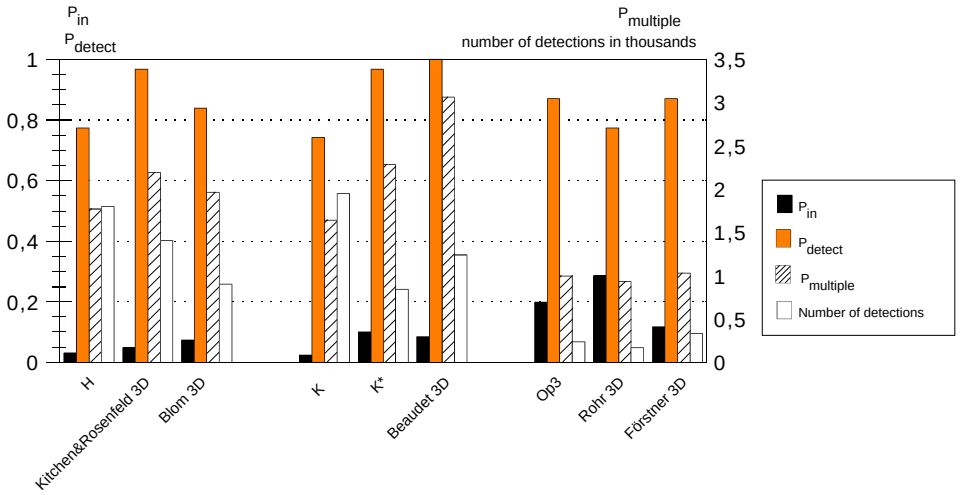

Figure 5. Detection performance of the nine investigated 3D operators for MR images.

means image volumes around the considered landmarks. From these studies it turns out, that the operators based on only first order partial derivatives of an image (*Op3*, *Rohr3D*, *Förstner3D*) yield the best results. Although the fraction of detected landmarks P_{detect} in Fig. 5, for example, is comparable for all operators, the fraction of correct detections P_{in} is significantly higher for the mentioned three operators. Additionally, the average number of multiple detections is $P_{multiple} \approx 1$ for these operators which is much better in comparison to the other operators (note the different units on the left and right side of the diagram). Out of the mentioned three operators, the operators *Op3* and *Rohr3D* show superior performance.

4.2. EVALUATION OF 3D MULTI-STEP PROCEDURES

Recently, we introduced multi-step differential approaches for 3D landmark extraction, combining landmark detection with additional steps for refined localization (Frantz et al. [10],[11]). As detection operators we utilize one of the operators *Op3*, *Rohr3D*, or *Förstner3D*. Subvoxel positions of the landmarks can be determined by applying a 3D extension of the 2D differential edge intersection approach of Förstner and Gülch [9]. With this extended approach, the 3D position estimate $\hat{\mathbf{x}}$ is determined by

$$\overline{\nabla g\ (\nabla g)^T}\ \hat{\mathbf{x}} = \overline{\nabla g\ (\nabla g)^T\ \mathbf{x}}, \tag{6}$$

where ∇g is the 3D image gradient and 'overline' means average. In summary, we have the following three multi-step procedures:
i) *Two-step procedure*: Application of a 3D detection operator of large and small scales for robust detection as well as refined localization.

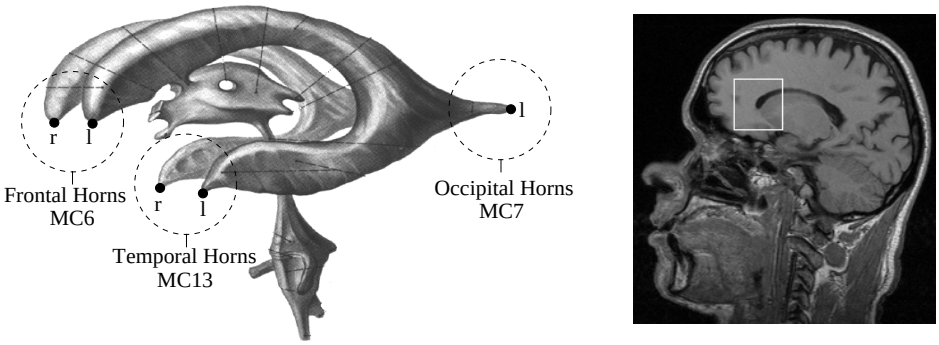

Figure 6. Ventricular system of the human brain adapted from [24] with marked landmarks (left), and frontal horn of the ventricular system in a 3D MR image (right).

ii) *Two-step procedure*: After landmark detection, the 3D differential edge intersection approach is applied. This procedure yields subvoxel positions and is the direct 3D extension of the two-step procedure in [9].
iii) *Three-step procedure*: Combination of the procedures i) and ii).

The multi-step procedures have been evaluated using 3D synthetic data and 3D MR images of the human head. In the latter case, we have considered as landmarks the tips of the frontal, occipital, and temporal horns of the ventricular system in three different MR data sets (see Fig. 6). The localization accuracy has been plotted in Fig. 7 separately for each landmark and for each MR image. We have computed the mean values $\overline{e}$ of the Euclidean distances from the localized positions to the manually specified positions, which we consider as 'ground-truth' (although we know that manual localization of 3D landmarks generally is difficult and may be prone to error). It can be seen that the multi-step procedures significantly improve the localization accuracy in comparison to applying a detection operator alone (DET). As detection operator we here applied the operator $Op3$. In the mean, the approaches i), ii) and iii) yield an improvement of $0.93vox$, $1.14vox$, and $1.52vox$ w.r.t. DET, resp., where vox denotes spatial unity. As an example, the localized positions for the tip of the left occipital horn have been visualized in Fig. 8 by three orthogonal sections of the 3D data.

5. Conclusions

We have described our studies on the validation and evaluation of 2D and 3D landmark operators. Our general approach consists of three main steps, (i) modelling the signal structure of landmarks, (ii) analysis of the degrees-of-freedom, and (iii) theoretical and experimental performance analysis. The formalization of the signal structure in our opinion is of paramount importance and is a key issue in the development of algorithms with pre-

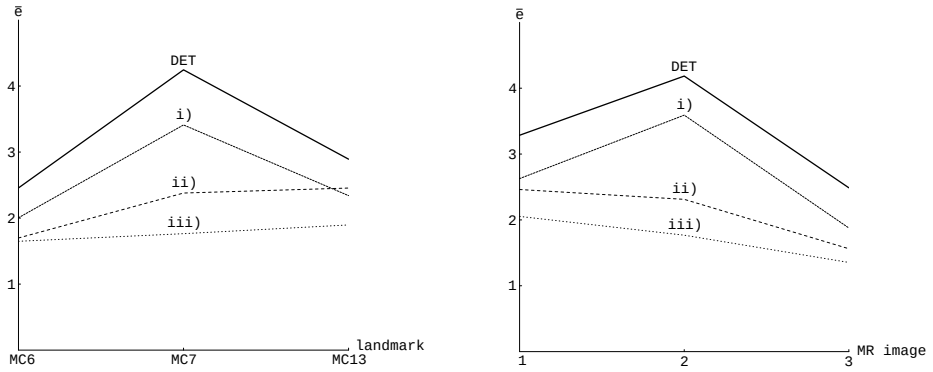

Figure 7. Mean localization accuracy $\overline{e}$ (mean of the Euclidean distances in voxel units to the manual positions) of the detection operator alone (DET) and the multi-step procedures i), ii), and iii) separately for each landmark (left) and for each MR image (right).

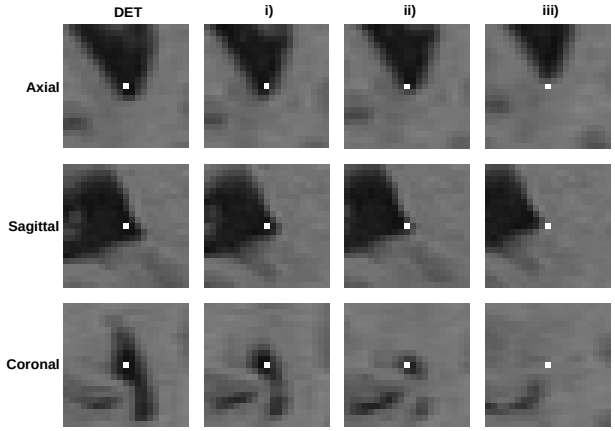

Figure 8. Localized positions for the tip of the left occipital horn of the ventricular system in a 3D MR image using the detection operator alone (DET) and the multi-step procedures i), ii), and iii) in axial, sagittal, and coronal views.

dictable performance. In the broader context of computer vision technology, our work is also relevant in the sense of shaping a methodology which allows to bridge the gaps between application problems, computational theories, and algorithms.

Acknowledgement

Support of Philips Research Hamburg, project IMAGINE (IMage- and Atlas-Guided Interventions in NEurosurgery), is gratefully acknowledged.

The tomographic image data have kindly been provided by Philips Research Hamburg, the AIM project COVIRA of the EU, the IMDM of the University Hospital Eppendorf (UKE) as well as W.P.Th.M. Mali, L. Ramos, and C.W.M. van Veelen (Utrecht University Hospital) via ICS-AD of Philips Medical Systems Best.

References

1. P.R. Beaudet, "Rotationally invariant image operators", *Proc. Intern. Joint Conf. on Pattern Recognition,* Kyoto/Japan, Nov. 7-10, 1978, 579-583
2. W. Beil, K. Rohr, and H.S. Stiehl, "Investigation of Approaches for the Localization of Anatomical Landmarks in 3D Medical Images", *Proc. Computer Assisted Radiology and Surgery (CAR'97),* Berlin, Germany, June 25-28, 1997, H.U. Lemke, M.W. Vannier, and K. Inamura (Eds.), Elsevier Amsterdam Lausanne 1997, 265-270
3. J. Blom, B.M. ter Haar Romeny, and J.J. Koenderink, "Affine invariant corner detection", submitted for publication, see "Topological and Geometrical Aspects of Image Structure", J. Blom, doctoral dissertation, University of Utrecht, May 1992
4. Coelho, C., Heller, A., Mundy, J.L., Forsyth, D.A. and Zisserman, A., "An Experimental Evaluation of Projective Invariants", *Geometric Invariance in Computer Vision,* J.L. Mundy and A. Zisserman (Eds.), The MIT Press, Cambridge, MA, 1992, 87-104
5. R. Deriche and G. Giraudon, "A Computational Approach for Corner and Vertex Detection", *Internat. J. of Computer Vision* 10:2 (1993) 101-124
6. L. Dreschler and H.-H. Nagel, "Volumetric Model and 3D-Trajectory of a Moving Car Derived from Monocular TV-Frame Sequences of a Street Scene", *Proc. IJCAI'81*, Vancouver, BC, 1981, 692-697, see also: *Computer Graphics and Image Processing* 20 (1982) 199-228
7. L.M.J. Florack, B.M. ter Haar Romeny, J.J. Koenderink, and M.A. Viergever, "General Intensity Transformations and Differential Invariants", *J. of Mathematical Imaging and Vision* 4 (1994) 171-187
8. W. Förstner, "A Feature Based Correspondence Algorithm for Image Matching", *Intern. Arch. of Photogrammetry and Remote Sensing* 26-3/3 (1986) 150-166
9. W. Förstner and E. Gülch, "A Fast Operator for Detection and Precise Location of Distinct Points, Corners and Centres of Circular Features", *Proc. ISPRS Intercomission Conf. on Fast Processing of Photogrammetric Data,* Interlaken/Switzerland, June 2-4, 1987, 281-305
10. S. Frantz, K. Rohr, and H.S. Stiehl, "Refined Localization of Three-Dimensional Anatomical Point Landmarks Using Multi-Step Differential Approaches", *Medical Imaging 1998 – Image Processing (MI'98),* Proc. SPIE Internat. Symposium, Vol. 3338, Part One, Febr. 23-26, 1998, San Diego/CA, K.M. Hanson (Ed.), 28-38
11. S. Frantz, K. Rohr, and H.S. Stiehl, "Multi-Step Procedures for the Localization of 2D and 3D Point Landmarks and Automatic ROI Size Selection", *Proc. European Conf. on Computer Vision (ECCV'98),* June 1998, Freiburg, Germany, Vol. I, *Lecture Notes in Computer Science* 1406, H. Burkhardt and B. Neumann (Eds.), Springer Berlin Heidelberg 1998, 687-703
12. T. Hartkens, K. Rohr, and H.S. Stiehl, "Evaluierung von Differentialoperatoren zur Detektion charakteristischer Punkte in tomographischen Bildern", *18. DAGM-Symposium Mustererkennung,* 11.-13. Sept. 1996, Heidelberg/Germany, *Informatik aktuell,* B. Jähne, P. Geißler, H. Haußecker, and F. Hering (Eds.), Springer-Verlag Berlin Heidelberg 1996, 637-644
13. T. Hartkens, K. Rohr, and H.S. Stiehl, "Performance of 3D differential operators for the detection of anatomical point landmarks in MR and CT images", *Medical Imaging 1999 – Image Processing (MI'99),* Proc. SPIE Internat. Symposium, Febr.

20-26, 1999, San Diego/CA, to appear
14. A. Heyden and K. Rohr, "Evaluation of Corner Extraction Schemes Using Invariance Methods", *Proc. 13th Internat. Conf. on Pattern Recognition (ICPR'96)*, Vienna, Austria, Aug. 25-29, Vol. I, IEEE Computer Society Press 1996, 895-899
15. L. Kitchen and A. Rosenfeld, "Gray-level corner detection", *Pattern Recognition Letters* 1 (1982) 95-102
16. H. Neumann and H.S. Stiehl, "Towards a Testbed for Evaluation of Early Vision Processes", *Proc. Internat. Conf. on Computer Analysis of Images and Patterns (CAIP'87),* Wismar, GDR, Sept. 2-4, 1987, L.P. Yaroslavskii, A. Rosenfeld, and W. Wilhelmi (Eds.), Akademie-Verlag Berlin 1987, 202-208
17. K. Rohr, "Untersuchung von grauwertabhängigen Transformationen zur Ermittlung des optischen Flusses in Bildfolgen", Diplomarbeit, Institut für Nachrichtensysteme, Universität Karlsruhe, 1987
18. K. Rohr, "Über die Modellierung und Identifikation charakteristischer Grauwertverläufe in Realweltbildern", *12. DAGM - Symposium Mustererkennung,* 24.-26. Sept. 1990, Oberkochen-Aalen, Germany, *Informatik-Fachberichte* 254, R.E. Großkopf (Hrsg.), Springer-Verlag Berlin Heidelberg 1990, 217-224
19. K. Rohr, "Recognizing Corners by Fitting Parametric Models", *Internat. J. of Computer Vision* 9:3 (1992) 213-230
20. K. Rohr, "Localization Properties of Direct Corner Detectors", *J. of Mathematical Imaging and Vision* 4:2 (1994) 139-150
21. K. Rohr, "On 3D Differential Operators for Detecting Point Landmarks", *Image and Vision Computing* 15:3 (1997) 219-233
22. K. Rohr and H.S. Stiehl, "Characterization and Localization of Anatomical Landmarks in Medical Images", *Proc. 1st Aachen Conf. on Neuropsychology in Neurosurgery, Psychiatry, and Neurology,* Dec. 12-14, 1997, Aachen/Germany, B.O. Hütter and J.M. Gilsbach (Eds.), Verlag der Augustinus Buchhandlung 1997, 9-12
23. C. Schmid, R. Mohr, and C. Bauckhage, "Comparing and Evaluating Interest Points", *Proc. Int. Conf. on Computer Vision (ICCV'98),* Bombay, India, Jan. 4-7, 1998, Narosa Publishing House, New Delhi Madras 1998, 230-235
24. J. Sobotta, *Atlas der Anatomie des Menschen, 1. Band,* H. Ferner and J. Staubesand (Eds.), Urban und Schwarzenberg, München Wien Baltimore 1988
25. J.-P. Thirion, "New Feature Points based on Geometric Invariants for 3D Image Registration", *Internat. J. of Computer Vision* 18:2 (1996) 121-137
26. O.A. Zuniga and R.M. Haralick, "Corner detection using the facet model", *Proc. IEEE Conf. on Computer Vision and Pattern Recognition,* Washington/D.C., June 19-23, 1983, 30-37